applied sciences

MDPI

Article

Monitoring and Analysis of Deformation Evolution Law of Fault Activation Caused by Deep Mining in Shizishan Copper Mine, China

Yanhui Guo * and Luo Luo

Faculty of Public Safety and Emergency Management, Kunming University of Science and Technology, Kunming 650093, China; luoluo@stu.kust.edu.cn

* Correspondence: guoyanhui0818@kust.edu.cn

Abstract: In order to study the deformation evolution law of fault activation caused by deep mining in Shizishan Copper Mine, China, a monitoring system for fault activation slip is designed and implemented on the basis of the field investigation of footwall fault activation of the main orebody in the mining area. The displacement and stress of the fault are monitored by the multipoint displacement meter, bolt stress meter, and borehole stress meter. According to the measured results, the activation deformation laws of fault F2, fault F3, and fault F4 during deep continuous mining are analyzed in detail. The results show that, when the influence range of underground mining spreads to the fault, the increase in the additional tensile stress on the fault plane will reduce the shear strength of the fault and increase the slip of the fault. When the shear stress exceeds the shear strength of the fault plane, the shear failure of the fault plane occurs, the rock mass on both sides of the fault loses stability, and the fault becomes active; when the orebody in the deep sublevel 14 and sublevel 15 were continuously stoped, the development of the mining influence area to fault F2 leads to fault F2's activation. When stoping the orebody in sublevel 16, fault F3 also activates. With the continuous downward mining of the deep part, the slip amount increases continuously. The fault activation sequence is from fault F2 to fault F3, and then to fault F4.

Keywords: steeply inclined orebody; deep mining; fault activation; monitor; deformation law

Citation: Guo, Y.; Luo, L. Monitoring and Analysis of Deformation Evolution Law of Fault Activation Caused by Deep Mining in Shizishan Copper Mine, China. *Appl. Sci.* **2022**, *12*, 6863. https://doi.org/10.3390/app12146863

Academic Editors: Hongyuan Liu, Tao Zhao and Bin Gong

Received: 26 May 2022
Accepted: 4 July 2022
Published: 7 July 2022

1. Introduction

With the rapid development of China's economy, the demand for mineral resources is also increasing gradually [1]. Complex geological conditions are often faced in underground mining. The difficulty of underground mining will increase with increases in mining depth and scope [2]. Faults are an inevitable main geological structure in underground mining, and their existence will destroy the continuity and stability of rock strata, thus changing the stress field and displacement field around the surrounding rock [3,4]. Fault activation may occur in the process of deep underground mining, which results in many mine disasters, such as rock burst [5], mine water inrush [6], and surface subsidence [7]. Therefore, fault activation has always been one of the important factors affecting the underground safety of mining [8]. Therefore, it is of great significance to analyze the deformation characteristics of fault activation in mining areas to prevent and control related disasters caused by fault activation.

In recent years, many scholars have carried out a lot of research on the deformation characteristics of fault activation. Most scholars have mainly focused on theoretical analysis [9–11], numerical simulation [12–14], and similar simulation experiments [15–17]. These three research methods mainly simulate and analyze the mechanical mechanism and activation process of fault activation, and then obtain the deformation characteristics of fault activation. However, the geological structure distribution of field faults is often complex; it is unavoidable to simplify the actual situation when analyzing through

theory, numerical simulation, and similar simulation experiments. The spatial and temporal deformation characteristics of fault activation are different from the actual situation. At present, there is relatively little monitoring of site fault activation, and most of the underground field monitoring is mainly microseismic monitoring. Chao Liu et al. [18] established a microseismic monitoring system and analyzed the activity of an excavation active interruption fault according to the monitoring results. Loginov G.N. et al. [19] discussed the optimization of microseismic monitoring in hard ore mining and developed a program to estimate the precision of microseismic monitoring. Kurlenya M.V. et al. [20] introduced the modeling process and calculation method of the wave field in anisotropic medium microseismic monitoring. Fuxing Jiang et al. [21] combined numerical simulation and microseismic monitoring to analyze the structure in underground mining. Baotang Shen et al. [22] monitored the stress state near the geological structure (e.g., faults and shear zones) of an underground coal mine in Australia. Ghosh G.K. et al. [23] monitored the stress state change in the geological structure of Rajendra underground coal mine in India to understand the change in stress distribution in the event of disasters and achieve safer mining operations. Wu Cai et al. [24] put forward the mechanical mechanism of fault activation dominated by the mine vibration load and the mechanism of dynamic and static load superposition-induced thrusting. Zhenhua Jiao et al. [25] studied the evolution law of fault damage and slip induced by mining in combination with on-site microseismic monitoring and orthogonal simulation tests. Shankun Zhao [26] comprehensively used acoustic emission monitoring, displacement, and stress monitoring to study the characteristics of overburden movement, ground pressure behavior and dynamic response before and after fault activation under the influence of mining. Bradley Forbes et al. [27] used multi-point rod extensometers, distributed optical fiber strand sensors, and borehole pressure cells (BHPCS) to measure and monitor the displacement and stress state changes of ore pillars. Narose H. et al. [28] built an underground mine monitoring system based on the Brillouin optical time domain reflectometer (BOTDR) system in El Teniente mine, and conducted field tests. Serdyukov S. et al. [29] introduced the engineering decision-making of microseismic data acquisition equipment to improve the information content of microseismic monitoring in the geodynamic process of underground hard ore mining.

In summary, for the study of fault activation monitoring, most scholars have focused on the problem of rock burst induced by fault activation, but ignored the fault displacement and stress changes in the process of fault activation. Few scholars have proposed analyzing a fault activation slip's spatial and temporal evolution characteristics through the field monitoring of fault displacement and stress. Based on the background of fault activation in the footwall of the main orebody induced by deep continuous mining in Shizishan mining area, Yuxi City, Yunnan Province, China, this paper designs a monitoring system suitable for fault activation and slip in this mining area in view of fault activation and slip. The displacement and stress of the fault are monitored by the multipoint displacement meter, bolt stress meter, and borehole stress meter. Through the field measurement of fault activation and slip, the stress and displacement evolution laws of the fault group activation process in the footwall of the main orebody during deep continuous mining are analyzed, and the spatiotemporal evolution characteristics of fault activation are discussed. The research results are significant for the research of fault activation monitoring methods caused by deep mining and the prevention and control of related disasters caused by fault activation.

2. Engineering Geology of Mining Area

Shizishan Copper Mine is located in Xiaojie township, Yimen county, Yunnan province, at the junction of the Yimen, Shuangbai, and Lufeng Counties. It is 51 km from Yimen county. Figure 1 shows the geographical location and regional structure outline of Shizishan Copper Mine. The south of the mining area is adjacent to the basin of fault Yuanjiang, the east is the Kunming depression belt, and the north is adjacent to the basin of fault Luwu. A set of strata have been deposited from Sinian, Paleozoic, to Mesozoic. The west of

the fault Lvzhijiang is the Yuanmou–Xinping ancient land, the Mesozoic red layer covers the upper part, and the basement is the Dahongshan group stratum. Within the scope of the mining area, the Kunyang group strata exposed accounted for more than 90%, only partially covered by Mesozoic red beds [30].

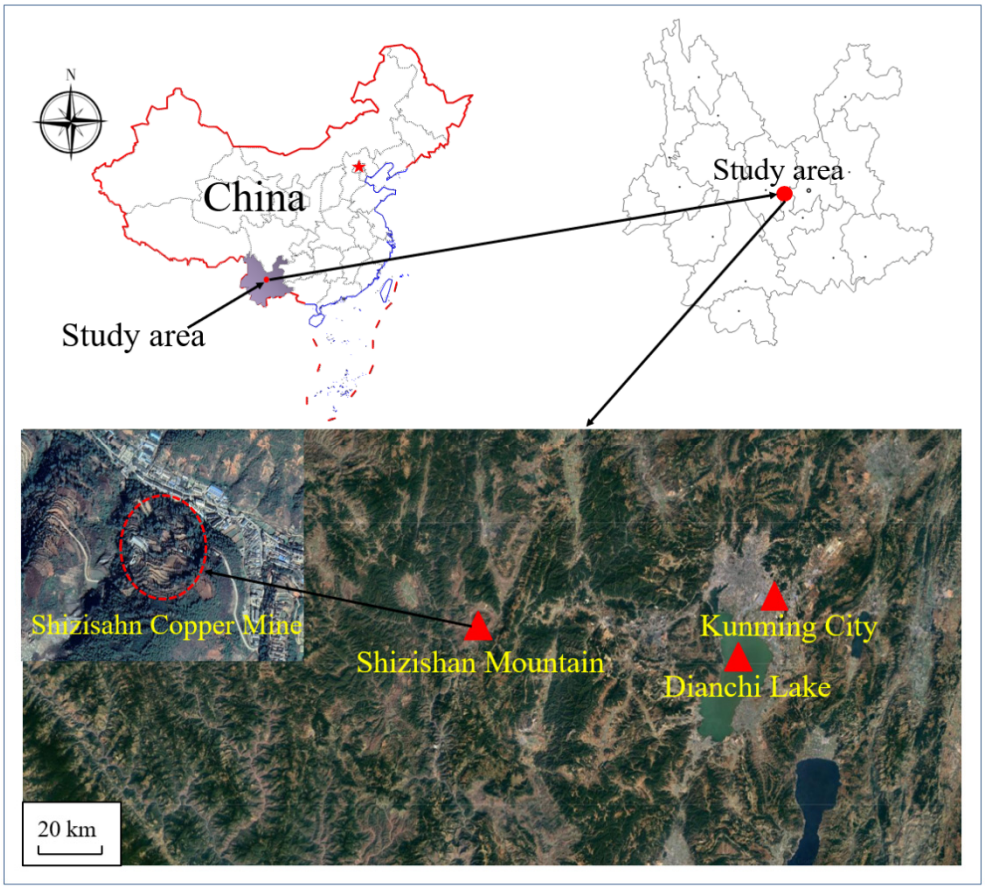

Figure 1. Position and regional structure outline of Shizishan Copper Mine.

The Kunyang group strata exposed in the mining area can be divided into seven groups, with a total thickness of more than 10,000 m. They are a set of shallow marine clastic rock formations and carbonate formations. The strata of each group from top to bottom are the Lvzhijiang formation, Etouchang formation, Luoxue formation, Yinmin formation, Meidang formation, Dalongkou formation, and Heishantou formation. The main lithologies of the mining area are Cyan grey dolomite, Faded dolomite, Purple slate, and Carbonaceous slate. The structure of the deposit is the same as the regional geological structure. The dominant fault group that has a great influence on deep mining is the NE longitudinal fault group, which is located in fault F2, fault F3 and fault F4 of the footwall of the main orebody. Fault F2 and F3 extend from sublevel 10 to sublevel 15, extending more than 200 m, of which the projects in sublevel 11 and sublevel 12 are relatively exposed more. Fault F4 extends from sublevel 6 to sublevel 18, which is a weak interlayer of Carbonaceous slate. The occurrence of each fault is shown in Table 1, and the geological engineering profile of each fault is shown in Figure 2.

Table 1. Parameter table of the main fault in the footwall of the main orebody of Shizishan Copper Mine.

Number of Fault	Trend (°)	Tendency (°)	Dip Angle (°)
F2	222	132	69
F3	221	131	71
F4	219	129	78

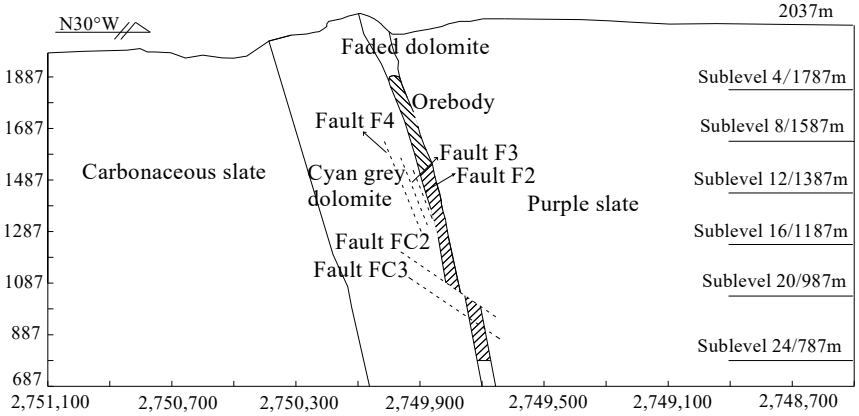

Figure 2. Engineering geological profiles of faults in Shizishan Copper Mine.

The dip angle of the orebody in Shizishan mining area is 70°–80°, which belongs to the steeply inclined orebody. The mine was put into operation in October 1977. The highest elevation of the mine's ground is 2143 m. The first-stage project is from sublevels 4 to 8, and the design elevation is 1807 m ~ 1587 m. The second-stage project is from sublevels 9 to 13; the design elevation is 1587 m ~ 1337 m, and the stoping is finished. The project's third phase is from sublevels 14 to 15, and the design elevation is 1337 m ~ 1237 m. The basic stoping of the third-phase project is completed. The fourth phase of the project is from sublevel 16 to 24, and the design elevation is 1237 m ~ 787 m.

3. Field Survey of Fault Activation Slip in Mining Area

Through the investigation of rock mass movement from sublevel 7 to sublevel 15 of the footwall of the main orebody in Shizishan mining area, we focused on determining the dominant faults that have an important impact on the stability of the project and selecting the appropriate monitoring points for the layout of the rock movement monitoring network. The investigation in April 2010 showed that the footwall of fault F2 had a great influence on the movement of rock mass. The maximum slip of fault F2 was 0.50 m. The deformation and failure of the roadway and chamber controlled by the fault are serious. With the overall subsidence of the hangingwall of the fault, many projects have been abandoned. However, fault F3 and fault F4 have not been activated, and fault FC2 and fault FC3 in the lower part of sublevel 18 have not been exposed. The field investigation in April 2015 showed that, during several years, under the influence of deep continuous mining, the slip of fault F2 continued to increase and reached about 1.6 m. Fault F3 has been activated under the influence of deep mining, the fault dislocation was obvious, and the slip amount was about 0.3 m. The faults in the footwall of the main orebody in the mining area are developing, and there are weak planes objectively, which create conditions for roadway deformation, cross-fall, collapse, and rock mass movement. Partial slip photos of fault F2 are shown in Figure 3 (April 2010).

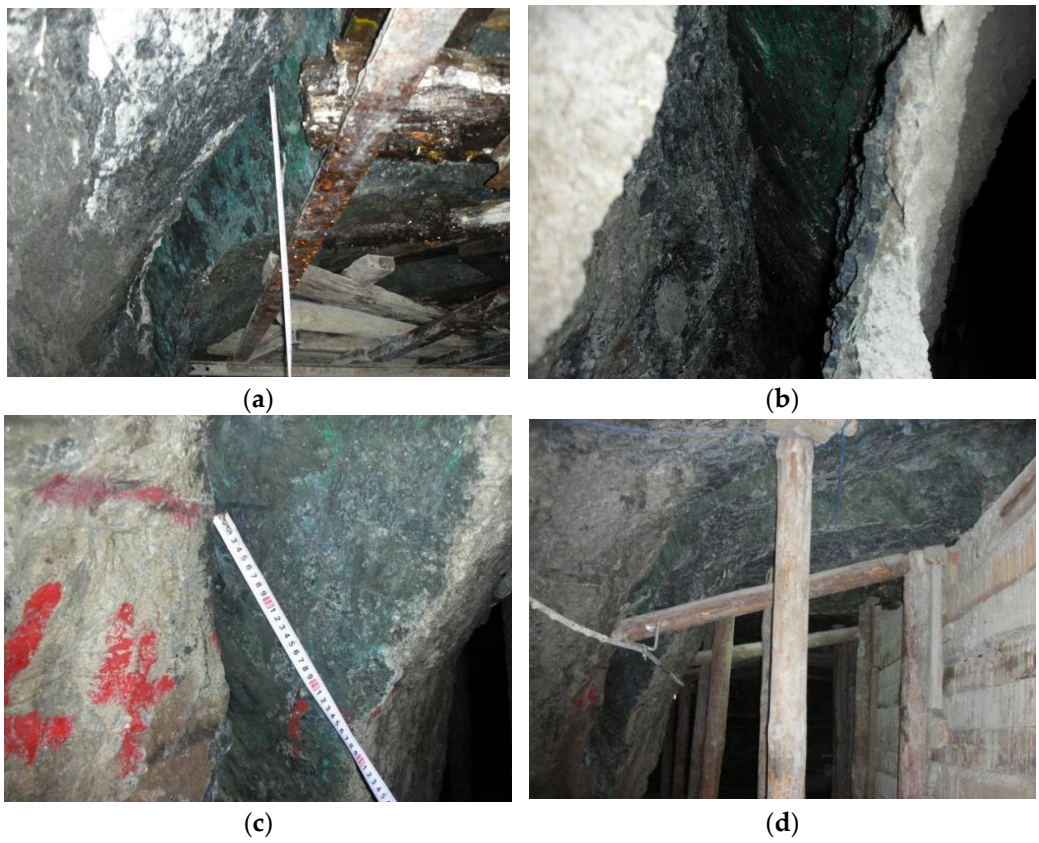

Figure 3. Partial slip photos of fault F2 (April 2010); they should be listed as: (**a**) The dislocation along the fault in the sublevel 12 roadway; (**b**) Fault movement along the fault in the bypass of sublevel 12's chute; (**c**) Sliding of the fault near the chute in the sublevel 12; (**d**) Fault dislocation of material chamber in sublevel 12.

4. Design of Fault Activation Slip Monitoring System

In order to explore the law of fault movement and failure in the process of deep continuous mining and its influence on the surrounding rock of the roadway, a monitoring system of fault activation slips was designed based on the field rock mass movement survey. Rock mass movement was mainly monitored for the displacement change in fault dislocation and the stress change in the surrounding rock in the hangingwall and footwall of the fault.

4.1. Monitoring Content

According to the actual situation of rock mass movement in the mining area, the monitoring content of underground rock mass movement was determined as follows: (1) during the mining process, the slip amount and variation laws of fault F2, fault F3, and fault F4 in the footwall of the main orebody were determined; and (2) the surrounding rock stress and its variation laws of the hangingwall and footwall of fault F2, fault F3, and fault F4 caused by mining were determined.

4.2. Monitoring Method

The monitoring of the fault is mainly based on the slip of the fault (dislocation displacement of the hangingwall and footwall of the fault), supplemented by stress monitoring. The multipoint displacement meter [31] is used to monitor the fault slip. Due to the large cumulative slip of the fault, the multipoint displacement measurement range is limited. When the slip exceeds the multipoint displacement measurement range, the marker line method is used to observe the displacement of the fault. The bolt stress meter and borehole stress meter [32,33] are used to observe the surrounding rock stress of the hangingwall

and footwall of the fault. The monitoring instrument adopts a vibrating wire multipoint displacement meter (monitoring precision is 0.01 mm), vibrating wire bolt stress meter (monitoring precision is 0.01 MPa), and vibrating wire borehole stress meter (monitoring precision is 0.01 MPa).

4.2.1. Monitoring Method of Fault Displacement Change

(1) Multipoint displacement monitoring method

The two-point multipoint displacement meter is used to monitor the dislocation displacement of the hangingwall and footwall of the fault. During installation, the sensor and the shorter anchor head are placed on the footwall of the fault so that, when the hangingwall of the fault moves towards the goaf, the shorter anchor head and the sensor remain relatively stationary, and the displacement measured by the longer anchor head is the fault dislocation displacement. Therefore, it is only necessary to read the displacement of the longer anchor head crossing the fault when measuring the displacement of fault dislocation. A schematic diagram of the installation of the multipoint displacement meter is shown in Figure 4.

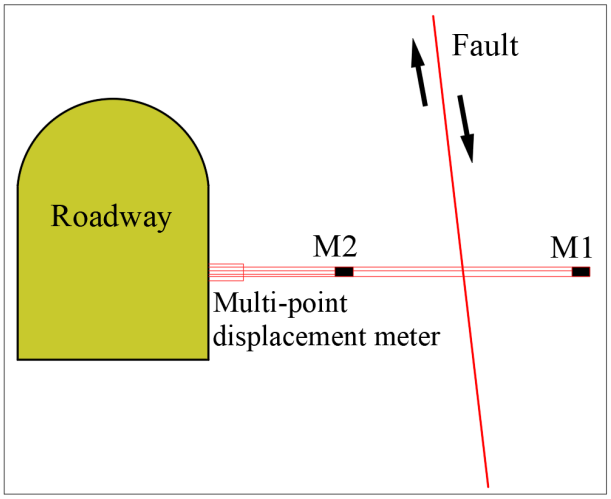

Figure 4. Installation diagram of the multipoint displacement meter.

(2) Mark line observation method

The mark line observation method is simple for field operation, convenient in application and can meet the observation requirements. When using this method, it is necessary to set up a marked observation line at the exposure of the fault on the roadway or chamber wall. When the fault slips, the marked line will slip along with the fault, and the marked observation line will move. The three-dimensional displacement of the staggered marked line on fault plane L is the actual slip amount of the fault. The schematic diagram of the mark line observation method is shown in Figure 5.

The relative increase in fault shear stress or the decrease in normal stress caused by mining may cause fault activation. However, according to the currently retrieved literature, there are few reports on an observation method for the fault stress state in the ground pressure activity and rock movement monitoring caused by underground mining. Therefore, this paper explores the observation method for the fault stress state and analyzes the variation law of the fault stress state in the mining process.

4.2.2. Monitoring Method of Fault Stress State

The change in the additional tensile stress perpendicular to the fault plane in the surrounding rock in the hangingwall and footwall of the fault was observed by using the bolt stress meter. During installation, the borehole was perpendicular to the fault plane,

and equal distance from the stress gauge in the surrounding rock of the hangingwall and footwall to the fault plane was kept. The distance selected in this paper was 2 m. The installation schematic of bolt stress meter is shown in Figure 6.

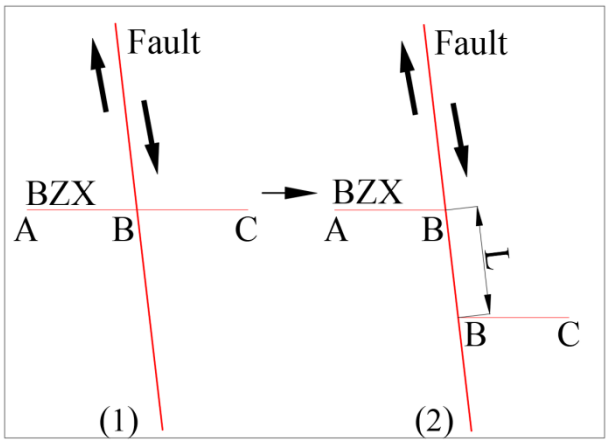

Figure 5. Schematic diagram of the mark line observation method.

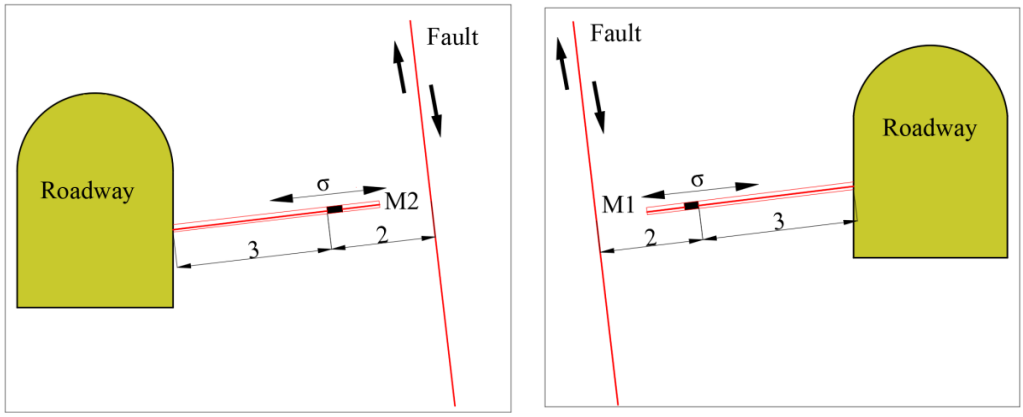

Figure 6. Installation diagram of the bolt stress meter, they should be listed as: (**a**) Installation schematic diagram of the bolt stress meter in the footwall of the fault; (**b**) Installation schematic diagram of the bolt stress meter in the hangingwall of the fault.

The variation of additional shear stress along the dip direction of fault plane in surrounding rock of hangingwall and footwall of fault was monitored by the borehole stress meter. The borehole was perpendicular to the fault plane, and equal distance from the stress gauge in the surrounding rock of the hangingwall and footwall to the fault plane was kept. The distance selected in this paper was 1 m. The installation diagram of borehole stress meter is shown in Figure 7.

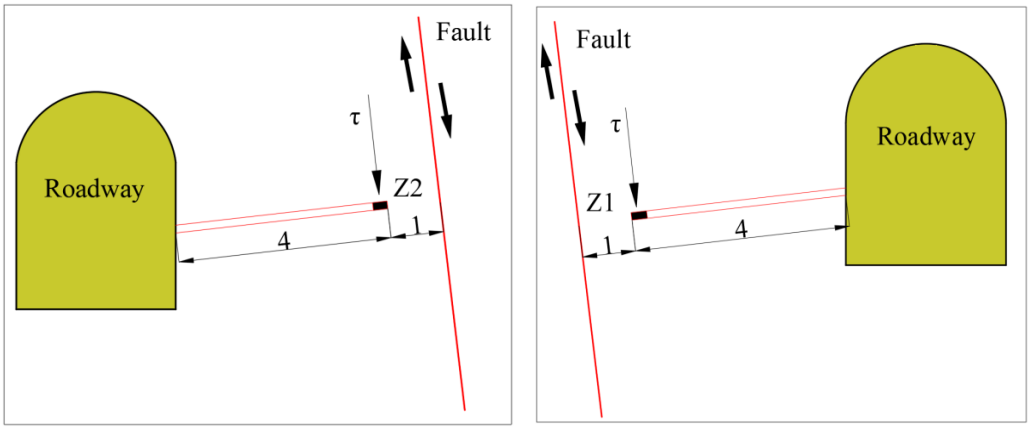

(**a**) (**b**)

Figure 7. Installation schematic diagram of the borehole stress meter, they should be listed as: (**a**) Installation diagram of the borehole stress meter in the footwall of the fault; (**b**) Installation schematic diagram of the borehole stress meter in the hangingwall of the fault.

4.3. Layout of Monitoring Points

A schematic diagram of the displacement and stress measuring points in each sublevel is shown in Figure 8. W is the multipoint displacement meter, BZX is the marked line monitoring point, M is the bolt stress meter, and Z is the borehole stress meter. In the multipoint displacement meter, the hole depth of monitoring points W11-6 is 12 m, and the spacing of the measuring points is arranged according to 4 m and 8 m, the hole depth of the other displacement meter is 4 m, and the spacing of the measuring points is arranged according to 1 m and 3 m. The borehole stress meter and bolt stress gauge depths are both 4 m. Photographs of some on-site monitoring instruments are shown in Figure 9.

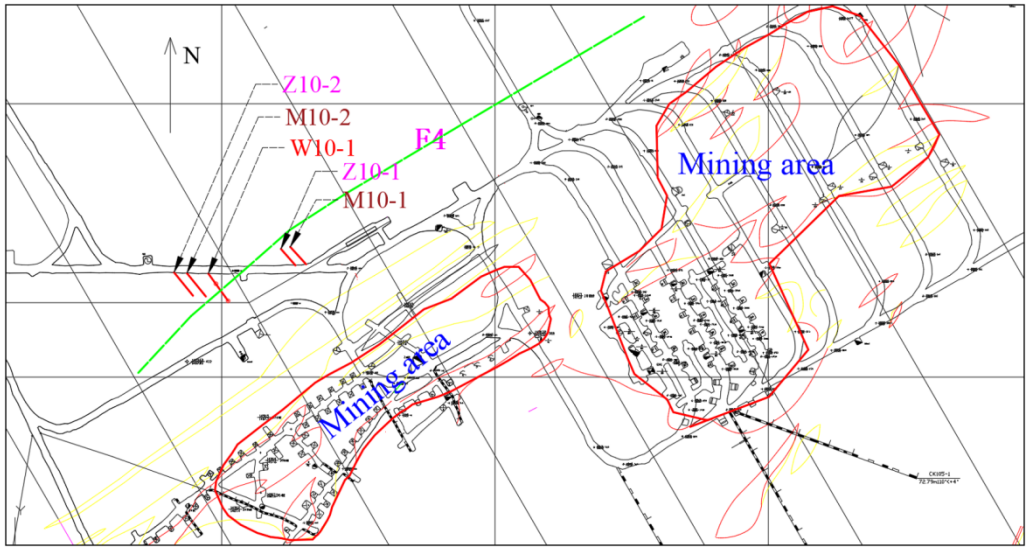

(**a**)

Figure 8. *Cont.*

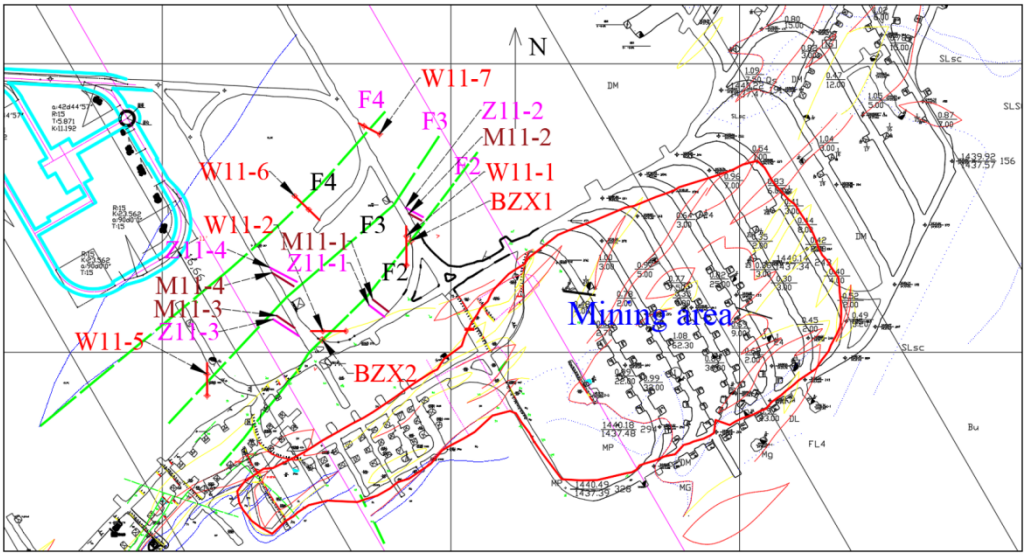

(**b**)

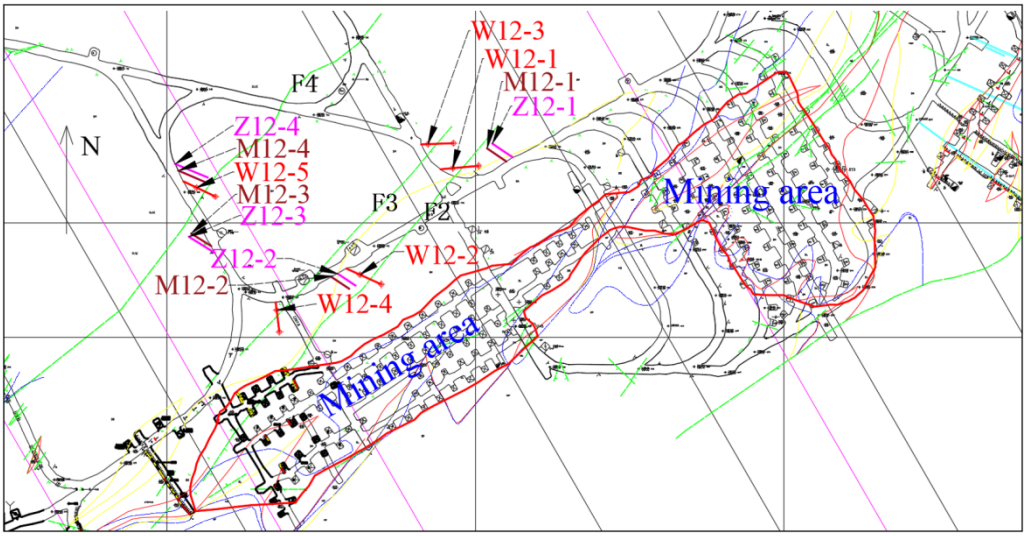

(**c**)

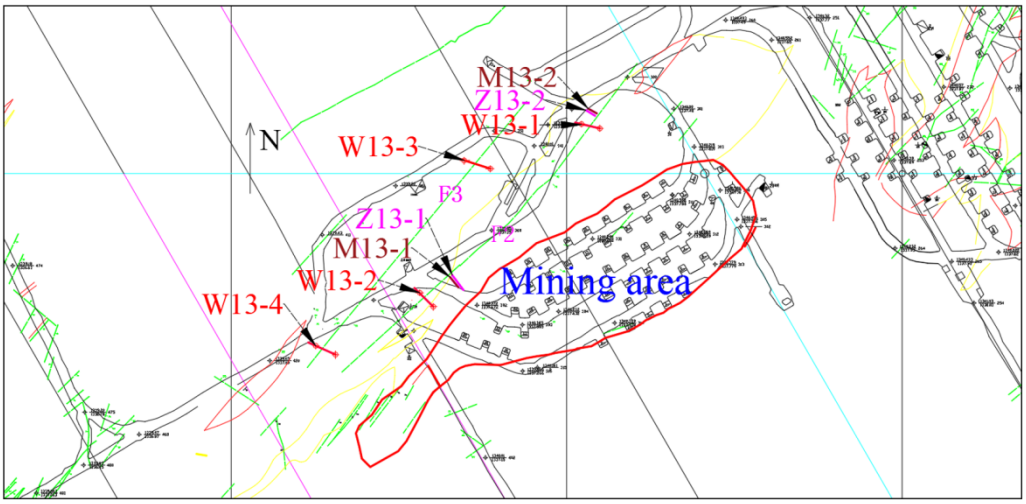

(**d**)

Figure 8. *Cont*.

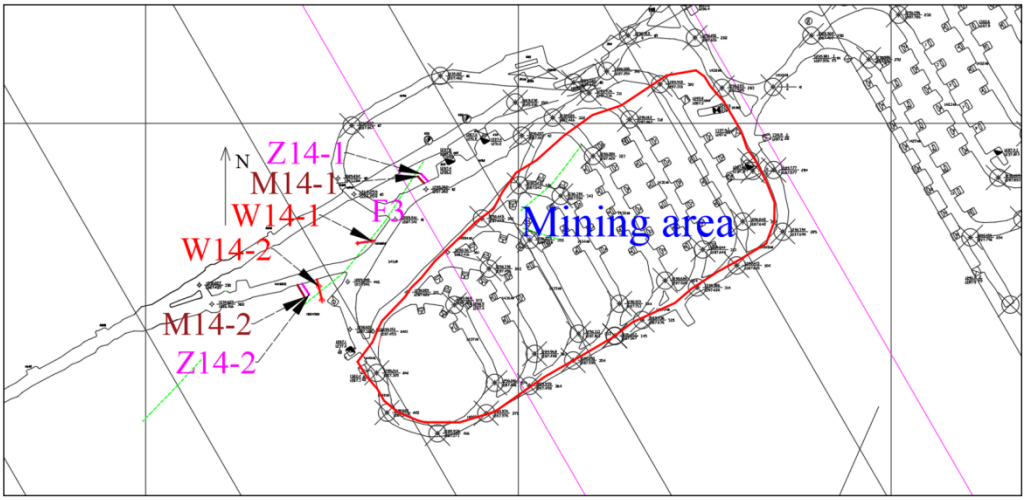

(**e**)

Figure 8. Schematic diagram of the arrangement of measuring points in each sublevel. (**a**) Measuring point position diagram of sublevel 10. (**b**) Measuring point position diagram of sublevel 11. (**c**) Measuring point position diagram of sublevel 12. (**d**) Measuring point position diagram of sublevel 13. (**e**) Measuring point position diagram of sublevel 14.

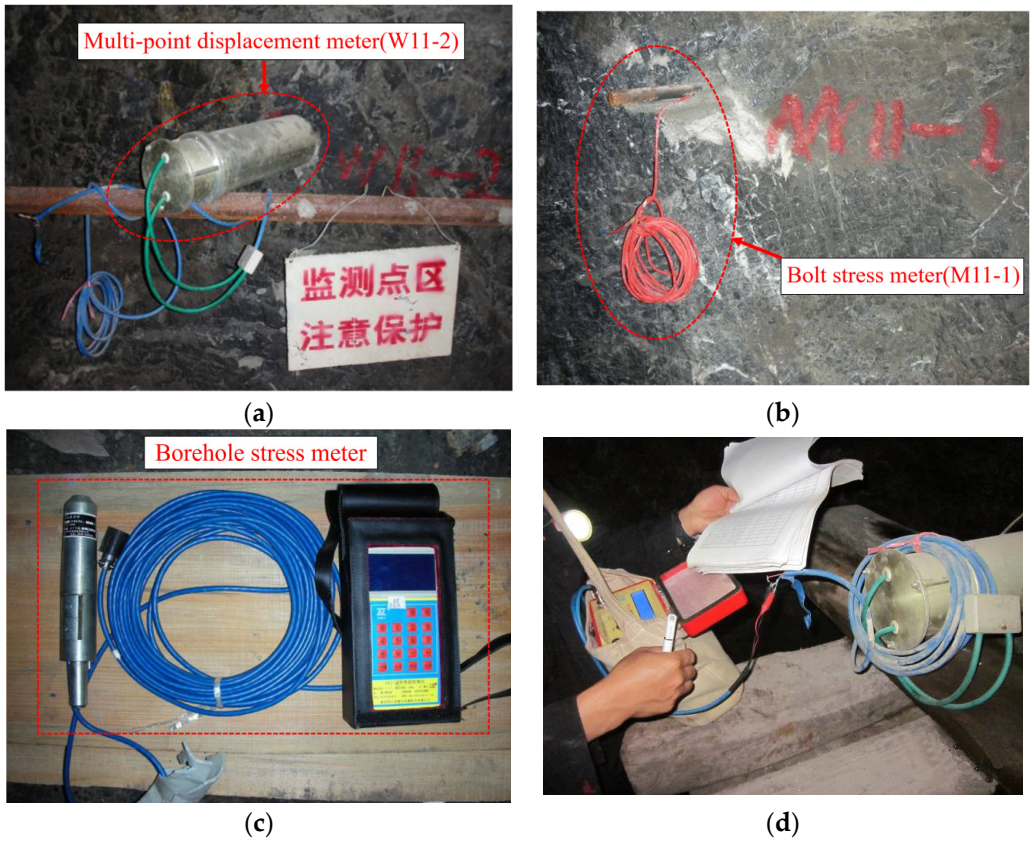

(**a**) (**b**)

(**c**) (**d**)

Figure 9. Photographs of the field monitoring instruments, they should be listed as: (**a**) On-site monitoring diagram of the multipoint displacement meter; (**b**) On-site monitoring diagram of the bolt stress meter; (**c**) On-site monitoring diagram of the borehole stress meter; (**d**) The author recording the monitoring data in the field.

5. Monitoring and Activation Law Analysis of the Fault Activation Slip

5.1. Displacement Analysis

5.1.1. Calculation Formula of Multipoint Displacement Meter

In the measurement process of the multipoint displacement meter, the displacement of the final fault dislocation can be calculated by Formula (1) [34,35].

$$P = K(F_i - F_0) \quad (1)$$

In the above formula: P—Displacement (mm);
K—Sensitivity coefficient of displacement meter (mm/F);
F_i—Frequency modulus at measurement (Frequency value ${F_i}^2 * 10^{-3}$);
F_0—Measured initial frequency modulus (Frequency value ${F_0}^2 * 10^{-3}$).

5.1.2. Analysis of Displacement Monitoring Data

According to the previous survey results, all faults to be monitored are normal faults. Therefore, this monitoring adopts two anchor head multipoint displacement meters. When installing the monitoring instrument, try to ensure that the multipoint displacement meter sensor and the shorter anchor head are located in footwall of the fault, and the deeper anchor head crosses the fault and is located in hangingwall of the fault. The results are processed based on the monitoring data; since the deep anchor head moves together with the fault during the movement of the hangingwall of the fault toward the goaf, the displacement measured by the deeper anchor head is the fault dislocation displacement, while the shorter anchor head and sensor are located in the footwall, which are relatively immobile, so the readings are within the normal error range and in the immobile state. Therefore, the displacement measured by the measuring point on the hangingwall of the fault crossing the fault is the fault slip displacement. The multipoint displacement meter monitoring curve of fault F2 is shown in Figure 10. Since 25 July 2011, the monitoring displacement of the multipoint displacement meter at each measuring point of fault F2 has gradually exceeded the range; therefore, after 25 July 2011, the observation of fault F2 was mainly conducted by the mark line observation method. The mark line measuring point is located in the exposed area of fault F2 in sublevel 12. Two points with better conditions are selected to set up the mark line observation. The data are read every three months. The slip of fault F2 observed by the marker line observation method is shown in Figure 11. Figures 12 and 13 show the multipoint displacement meter monitoring curve of fault F3 and fault F4, respectively. The monitoring period was from November 2010 to April 2015. The mining elevation is from sublevel 14 to the end of sublevel 15, and the stoping of deep orebody in sublevel 16 and the development of sublevel 17 are currently underway. The main results of the observation are as follows:

(1) As of 25 July 2011, the cumulative displacement of each measuring point for monitoring fault F2 is: W11-1 is 291.2 mm, W11-2 is 332.3 mm, W12-1 is 350.4 mm, W12-2 is 374.1 mm, W13-1 is 385.3 mm, and W13-2 is 400.5 mm. During the monitoring period, the average cumulative movement of fault F2 is 355.6 mm, and the average movement rate is 1.36 mm/d. As of 14 April 2015, the fault F2 mark line monitoring, cumulative fault slip of measuring point BZX1 is 1.45 m, and the cumulative fault slip of measuring point BZX2 is 1.56 m. The cumulative slip of each measuring point of fault F3 is: W11-5 is 21.33 cm, W12-3 is 22.13 cm, W12-4 is 25.16 cm, W13-3 is 25.188 cm, W13-4 is 27.00 cm, W14-1 is 27.26 cm, and W14-2 is 27.27 cm. The displacement values of each measuring point used for monitoring fault F4 are as follows: W10-1 is 0.021 mm, W11-6 is 0.024 mm, W11-7 is 0.038 mm, and W12-5 is 0.072 mm.

(2) From the trend of the slip–time curves of the three faults, the moving rate of fault F2 is relatively large. After the fault activation under the influence of deep mining, the cumulative slip is the largest, reaching 1.56 m. Fault F3 has also activated and slipped under the influence of mining, and the cumulative displacement of the measuring point with a large slip is 27.27 cm. The measuring point with the largest displace-

ment of fault F4 is W11–6, and the displacement is 0.072 mm. The displacement value is small and within the normal error range, indicating that fault F4 has not been activated.

(3) According to the monitoring results, during the same monitoring time, the monitoring displacement of the multipoint displacement meter in the lower sublevel is greater than that in the upper sublevel, and the displacement of the measuring point near the goaf is greater than that far away from the goaf, indicating that the movement of the fault propagates from the bottom to the top. From nearby to far away from the goaf, the fault activation sequence is from fault F2 to fault F3, and then to fault F4. In general, for fault F2, at the same monitoring time, the displacement of the measuring point on the west side of the fault is greater than that on the east side of the fault. For example, the displacement of measuring point W11-2 is greater than that of W11-1, the displacement of measuring point W12-2 is greater than that of W12-1 and the displacement of measuring point W13-2 is greater than that of W13-1, indicating that, in the process of moving the hangingwall of fault F2 to the goaf, there is also a rotation along the right direction of the fault. The main reason is that the west side is closer to the mining area.

(4) From the monitoring results, the dislocation displacement of fault F2 and fault F3 has a sudden increase during the monitoring time; it is especially obvious in the monitoring data of fault F2. Compared with the observation time of the large displacement change and stope blasting time, it can be learned that the point of time of the sudden increase in the large displacement is the large blasting time or a short time after blasting. This indicates that large underground blasting has a certain influence on fault activation dislocation.

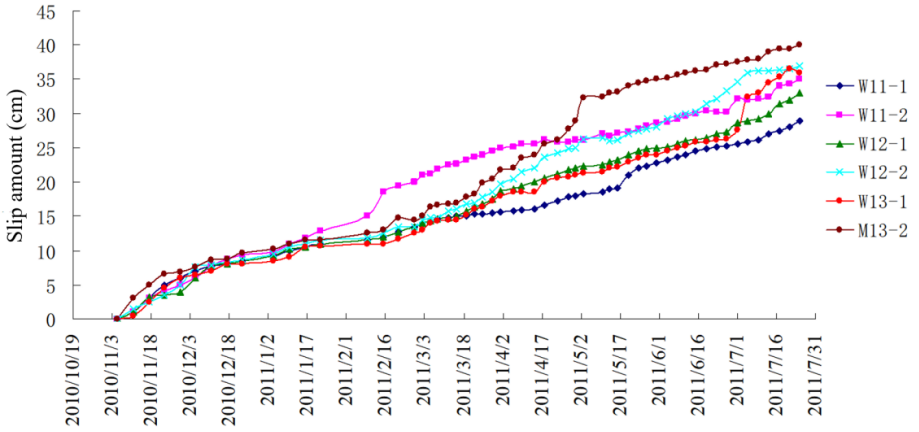

Figure 10. Multipoint displacement meter monitoring displacement–time curve of each measurement point of fault F2.

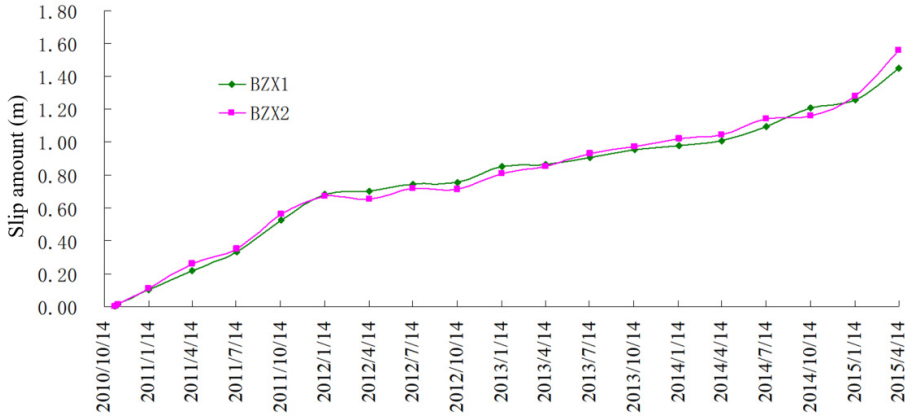

Figure 11. Slip–time monitoring curve of fault F2 observed by the mark line.

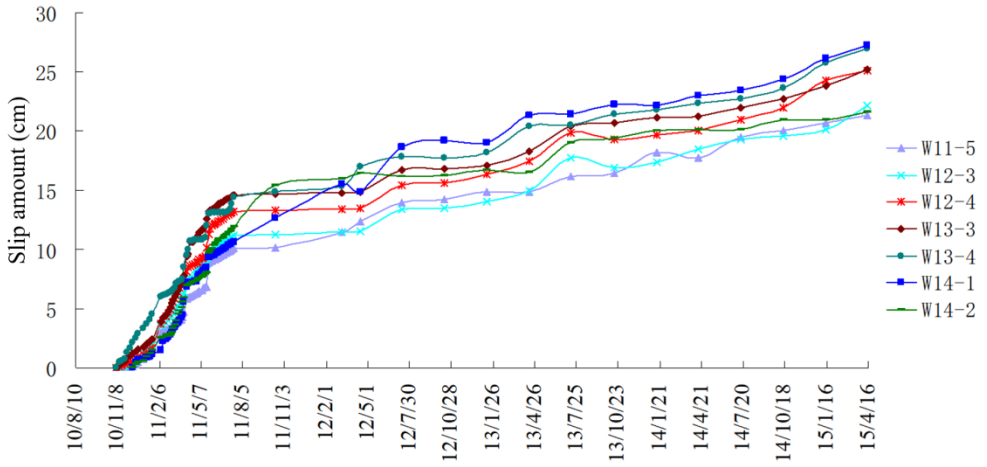

Figure 12. Multipoint displacement meter monitoring displacement–time curve of each measurement point of fault F3.

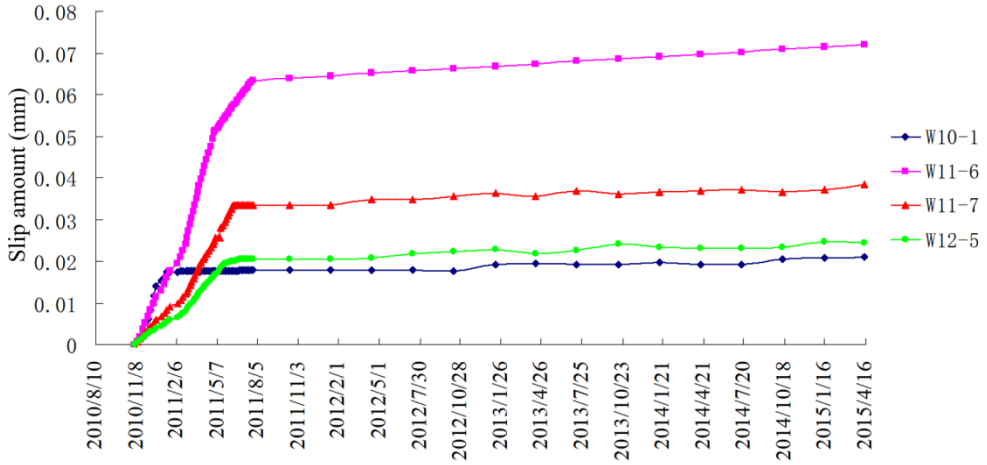

Figure 13. Multipoint displacement meter monitoring displacement–time curve of each measurement point of fault F4.

5.2. Stress Analysis

5.2.1. Analysis of Monitoring Results of the Bolt Stress Meter

(1) Computing formula

In the measurement process of the bolt stress meter, the stress of the surrounding rock around the final fault can be calculated by Formula (2) [35].

$$P = \frac{P'}{A} = \frac{S * \left(f_i{}^2 - F_0{}^2\right)}{A} \quad (2)$$

In the above formula:
P—Stress on the measured bolt stress meter (MPa);
A—Cross-sectional area of the measured bolt stress meter (m^2);
P'—The force on the measured bolt stress meter (kN);
S—Sensitivity coefficient of the bolt stress meter (kN/Hz^2);
F_0—Initial frequency of the bolt stress meter;
f_i—Working frequency of the bolt stress meter.

(2) Analysis of monitoring results of the bolt stress meter

If the frequency of the bolt stress meter reading instrument increases, the calculated results are positive under tension force. The frequency of the readout is decreased, and the

calculation results are negative under compressive stress force. According to the actual situation of tension and compression, different sensitivity coefficients were used to calculate the stress measured at each measuring point. According to the installation diagram of the bolt stress meter in Figure 5, the measured stress of the bolt stress meter is the change in the additional stress of the rock mass near the fault plane perpendicular to the fault plane. The stress curve of each measuring point with time is shown in Figures 14–16.

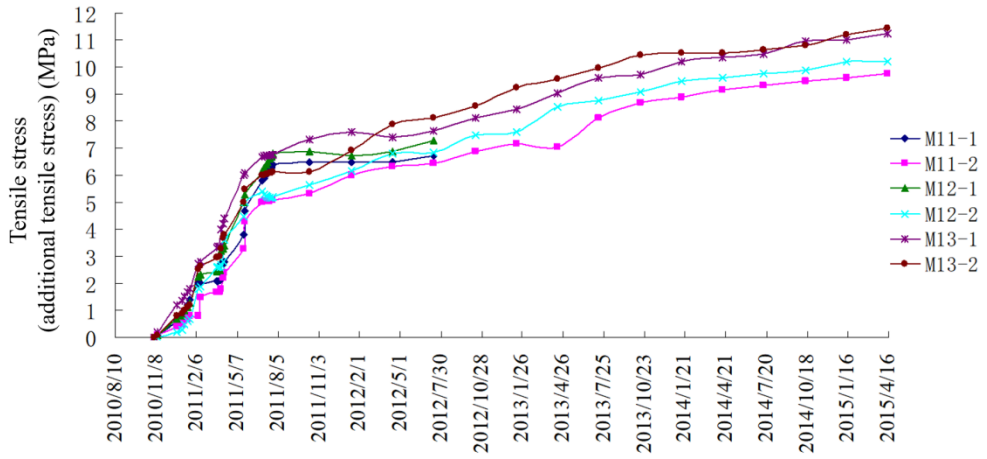

Figure 14. The stress–time curve of each measuring point of fault F2 monitored by the bolt stress meter.

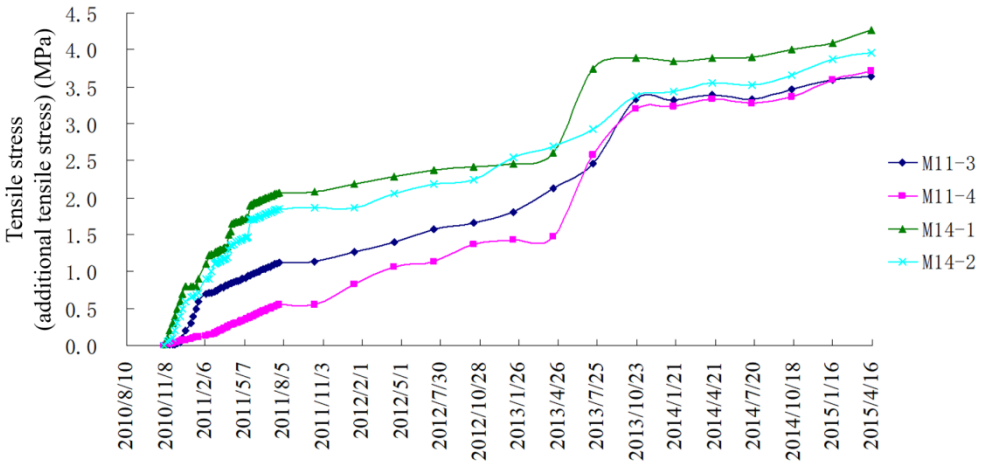

Figure 15. The stress–time curve of each measuring point of fault F3 monitored by the bolt stress meter.

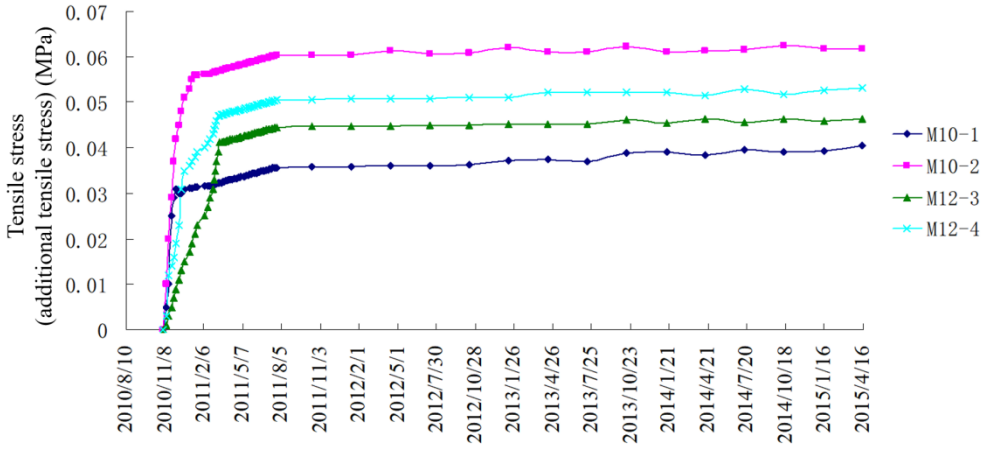

Figure 16. The stress–time curve of each measuring point of fault F4 monitored by the bolt stress meter.

(1) As of 14 April 2015, the stress values of each measuring point used to monitor fault F2 are as follows: M11-2 is 9.77 MPa, M12-2 is10.20 MPa, M13-1 is 11.24 MPa, and M13-2 is 11.44 MPa. Due to the damage near measuring points M11-1 and M12-1, the readings of these two measuring points are those as of 14 July 2012. During the monitoring period, the average tensile stress of the hangingwall of fault F2 perpendicular to fault plane 2 m is 6.65 MPa, and the average tensile stress of the footwall of fault F2 perpendicular to fault plane 2 m is 5.46 MPa. The stress values of each measuring point for monitoring fault F3 are: M13-3 is 3.64 MPa, M13-4 is 3.72 MPa, M14-1 is 4.27 MPa, and M14-2 is 3.96 MPa. The stress of each measuring point of fault F4 is within the initial error range, and the change is small.

(2) The calculation shows that, with the continuous deep mining, the additional tensile stress of the surrounding rock of the hangingwall and footwall of faults F2 and F3 is vertical to the fault plane and increases over time; the stress of fault F4 changes little. Through data analysis and the comparison of the changes in the additional tensile stress of each measuring point on the hangingwall and footwall of the fault at the same time, it is found that the additional tensile stress in the hangingwall of the fault is greater than that in the footwall of the fault at the same fault, indicating that the existence of the fault has a certain barrier effect on the stress distribution.

(3) Comparing the three monitoring times with large stress variation values and the large blasting time of the stope, after the large blasting operation was carried out in the stope of sublevel 15 of the footwall of the main orebody, the stress value increases rapidly, indicating that the blasting operation has a great influence on the stress distribution in the fault and surrounding rock. It also indicates that the stress in the orebody and surrounding rock change significantly under the influence of mining, and the ground pressure activity enhances significantly.

5.2.2. Analysis of Monitoring Results of the Borehole Stress Meter

After the borehole stress meter is installed, the frequency value and the compressive stress in the borehole aperture direction can be read directly on the reader. According to the schematic diagram of the borehole stress meter installation in Figure 6, the stress measured by the borehole stress meter is the compressive stress in the direction of the borehole aperture; that is, the variation in the additional shear stress of the rock mass located on the hangingwall and footwall of the fault plane along the dip direction of the fault plane. The variation curves of the compressive stress with time at each measuring point are shown in Figures 17–19.

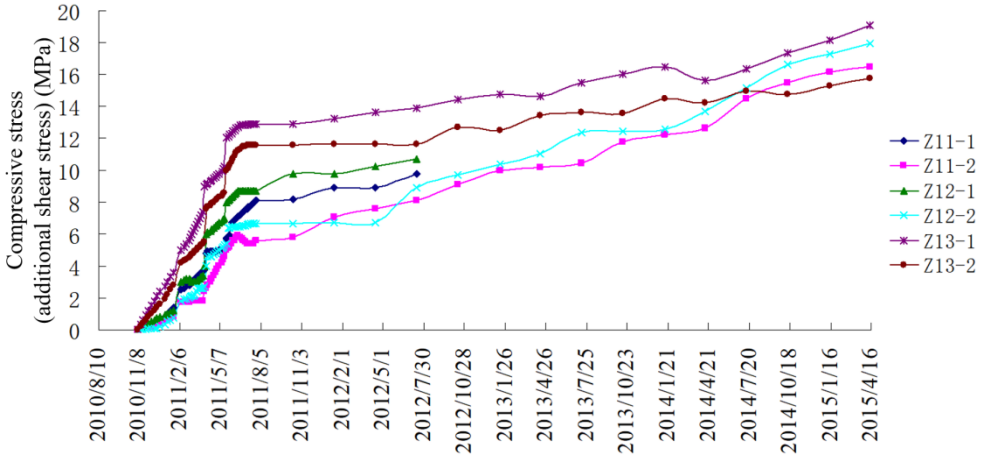

Figure 17. The stress–time curve of each measuring point of fault F2 monitored by the borehole stress meter.

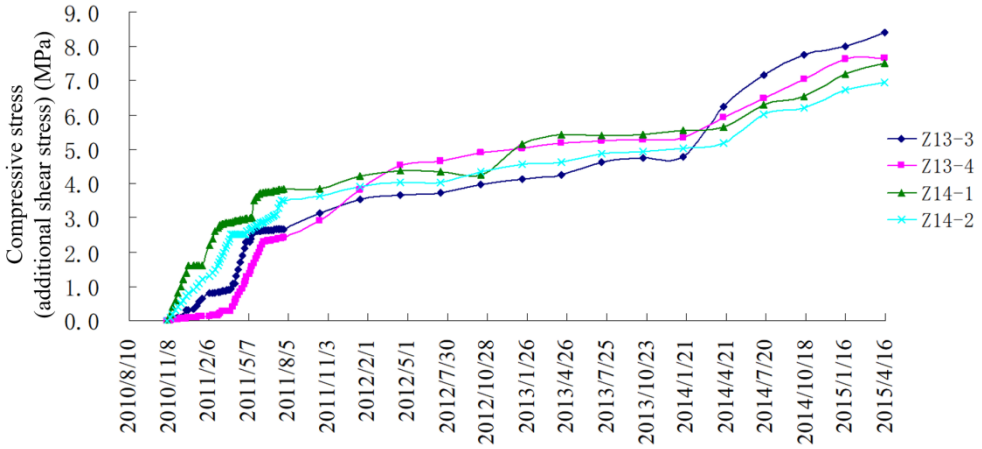

Figure 18. The stress–time curve of each measuring point of fault F3 monitored by the borehole stress meter.

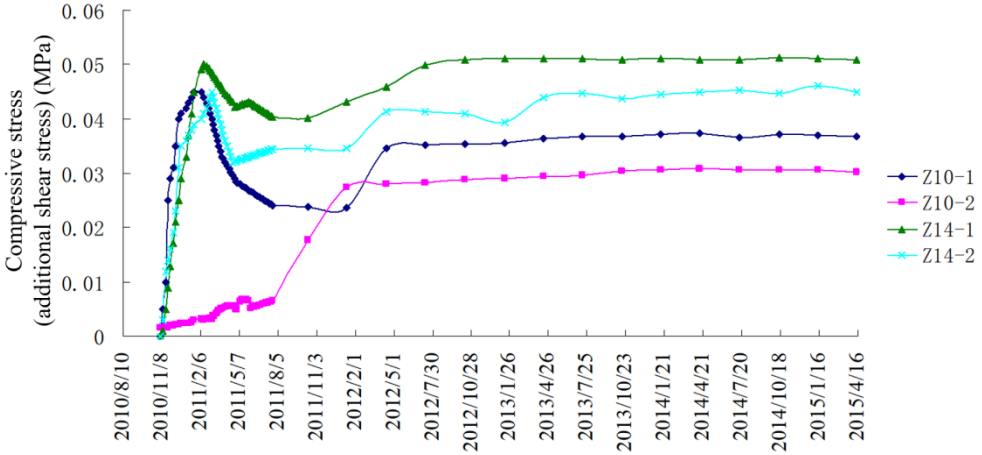

Figure 19. The stress–time curve of each measuring point of fault F4 monitored by the borehole stress meter.

(1) As of 14 April 2015, the stress values of each measuring point used for monitoring fault F2 are as follows: Z11-2 is 16.50 MPa, Z12-2 is 17.96 MPa, Z13-1 is 19.04 MPa, and Z13-2 is 15.75 MPa. Due to the damage near the measuring point, the readings of Z11-1 and Z12-1 are those as of 14 July 2012. The stress values of each measuring point used for monitoring fault F3 are as follows: Z13-3 is 8.41 MPa, Z13-4 is 7.67 MPa, Z14-1 is 7.50 MPa, and Z14-2 is 6.95 MPa. The stress of each measuring point of fault F4 did not change greatly.

(2) From the calculation results, it can be seen that, with the continuous deep mining, additional shear stress along the fault plane is generated in the surrounding rock of the hangingwall and footwall of fault F2 and fault F3 and increases gradually over time, while the stress of fault F4 changes little and is within the error range. Through data analysis, compared with the change in the additional shear stress of each measuring point in the hangingwall and footwall of the fault at the same time, it is found that the additional shear stress of the hangingwall of the fault is greater than that of the surrounding rock of the footwall of the fault, indicating that the existence of the fault has a certain barrier effect on the stress distribution. The change in the additional shear stress at the monitoring point on the west side of the fault is greater than that on the east side, indicating that the influence of mining on the west side of the fault is greater than that on the east side—the main reason for this is that the mining area in the west is closer to the fault.

(3) Comparing the bolt stress meter and borehole stress meter at the same monitoring position of fault F2, it can be found that the additional shear stress generated by the same monitoring position of the fault is greater than the additional tensile stress within the same time.
(4) Comparing the monitoring time with an abrupt change in the stress value and the large blasting time of stope, it can be found that the stress value increases rapidly after the large blasting operation, indicating that the blasting operation has a certain influence on the additional shear stress along the dip direction of the fault plane.

5.3. Regularity Analysis of Fault Activation Slip Based on Monitoring Results

According to the monitoring data of fault activation dislocation displacement for more than four and a half years and the monitoring results of stress change in the surrounding rock of the hangingwall and footwall of the fault, the following conclusions can be drawn by comprehensive analysis:

(1) From the relative relationship between the fault and the location of the mining area and the slip failure of the fault, it can be concluded that fault F2, fault F3, and fault F4 in the footwall of the main orebody are normal faults; that is, the hangingwall of the fault has moved to the goaf or there is a trend to move to the goaf. Under the influence of deep mining, the normal stress on fault F2's and fault F3's planes decreases, and the shear strength decreases. When the shear stress is greater than the shear strength, movement and failure to the goaf will occur.
(2) During the mining of the orebody in sublevel 14 and sublevel 15, fault F2 was activated as the mining influence area developed to fault F2. With the passage of time, the slip amount of fault F2 gradually increased, and the cumulative slip amount reached 1.56 m. In the process of mining the orebody in sublevel 16 of the deep part, the mining influence range is spread to fault F3, and fault F3 is also activated. At present, the place with the largest accumulative slip amount is 27.27 cm, and with the continuous downward mining in the deep part, the slip amount is increasing. The monitoring data showed that activation dislocation did not occur at fault F4, indicating that the mining influence range did not reach fault F4.
(3) From the monitoring data results, in the same monitoring time, the monitoring displacement of the multipoint displacement meter in the lower sublevel is greater than that in the upper sublevel, and the displacement of the measuring point near the goaf is greater than that far from the goaf, indicating that the movement of the fault is transmitted from bottom to top, and the distance from the mining area is developed from near to far. The fault activation sequence is from fault F2 to fault F3 and then to fault F4. In addition, for fault F2, at the same monitoring time, the displacement of the measuring point on the west side of the fault is larger than that on the east side of the fault, indicating that the rotation of the hangingwall of fault F2 along the right direction of the fault occurs in the process of moving to the goaf. From the stress–displacement curve with time combined with the large blasting time of the footwall of the main orebody, it can be concluded that blasting vibration has a certain influence on the fault activation.
(4) From the stress monitoring results, when the mining influence range spreads to the fault, additional tensile stress perpendicular to the fault plane and additional shear stress along the dip direction of the fault plane are produced in the surrounding rock of the hangingwall and footwall of the fault and increase with the increase in the mining influence range. At the same monitoring position, the additional shear stress is greater than the additional tensile stress, and the stress change value of the surrounding rock of the hangingwall of the fault is greater than that of the footwall, indicating that the existence of the fault has a certain barrier effect on the propagation of stress. It also shows that, when the influence range of underground mining affects the fault, the increase in additional tensile stress on the fault plane will reduce the shear strength of the fault and increase the slip of the fault. When the shear stress exceeds the shear

strength of the fault plane, shear failure occurs on the fault plane, and the rock mass on both sides of the fault loses stability, resulting in small dislocation or overall slip, which is the essence of fault F2's and fault F3's activation. From the monitoring results, fault F4 has not yet been activated.

(5) According to the activation slip of the fault, the movement of the surrounding rock of the hangingwall of fault F2 will lead to a decrease in the confinement effect of the surrounding rock of the hangingwall of the fault on the surrounding rock of the footwall. The surrounding rock of the footwall of fault F2 is the surrounding rock of the hangingwall of fault F3. When the confinement effect of the surrounding rock of the hangingwall fault of F2 on the surrounding rock of the footwall is small to enough, the hangingwall of fault F3 will also move in the direction of the goaf, and the movement of fault F3 to a certain extent may also lead to the dislocation of fault F4. Therefore, the footwall of the main orebody is controlled by the dominant fault, and the movement and destruction of the fault conform to the domino effect.

6. Conclusions

(1) When sublevel 14 and sublevel 15 are continuously mined in the deep part of the main orebody, the mining influence range spreads to fault F2, and fault F2 is activated. With the passage of time, the slip increases gradually. In the process of mining the deep orebody of sublevel 16, the mining influence range spreads to fault F3, and fault F3 is also activated. As the deep mining continues downward, the slip amount is increasing. During the monitoring period, fault F4 did not generate activation dislocation.

(2) Within the same monitoring time, the monitoring displacement of the multipoint displacement meter in the lower sublevel is greater than that in the upper sublevel, and the displacement of the measuring point near the goaf is greater than that far from the goaf, indicating that the movement of the fault is transmitted from bottom to top, and the distance from the mining area is developed from near to far. The fault activation sequence is from fault F2 to fault F3, and then to fault F4. Moreover, for fault F2, at the same monitoring time, the displacement of the measuring point on the west side of the fault is larger than that on the east side of the fault, indicating that the hangingwall of fault F2 also rotates along the right direction of the fault in the process of moving to the goaf; the main reason for this is that the west side is closer to the mining area.

(3) When the mining influence range spreads to the fault, additional tensile stress perpendicular to the fault plane and additional shear stress along the dip direction of the fault plane are produced in the surrounding rock of the hangingwall and footwall of the fault. The additional tensile stress increases with the increase in the mining influence range. At the same monitoring position, the additional shear stress is greater than the additional tensile stress, and the stress change value of the surrounding rock of the hangingwall of the fault is greater than that of the footwall, indicating that the existence of the fault has a certain barrier effect on the propagation of stress. When the influence range of underground mining affects the fault, the increase in additional tensile stress on the fault plane will reduce the shear strength of the fault and increase the slip of the fault. When the shear stress exceeds the shear strength of the fault plane, the fault plane will undergo shear failure, and the rock mass on both sides of the fault will lose stability, resulting in small dislocation or overall slip, which is also the essence of fault F2's and fault F3's activation.

Author Contributions: Conceptualization: Y.G.; methodology: Y.G. and L.L.; formal analysis: Y.G. and L.L.; writing—Original draft: Y.G.; writing—Review and editing: Y.G. and L.L.; resources: Y.G.; funding acquisition: Y.G.; validation: Y.G. and L.L. All authors have read and agreed to the published version of the manuscript.

Funding: This research was funded by the Scientific Research Fund Project of Yunnan Provincial Department of Education, China (no. 2022J0065); Key Projects of Analysis and Testing Fund of Kunming University of Science and Technology, China (no. 2021T20200145); China Postdoctoral Science Foundation Project (no. 2017M620433); and General Projects of Yunnan Fundamental Research Projects (no. 2018FB075).

Institutional Review Board Statement: Not applicable.

Informed Consent Statement: Not applicable.

Data Availability Statement: Not applicable.

Conflicts of Interest: The authors declare no conflict of interest.

References

1. Xie, H.P. Research framework and anticipated results of deep rock mechanics and mining theory. *Adv. Eng. Sci.* **2017**, *49*, 1–16.
2. Kong, P.; Jiang, L.S.; Shu, J.M.; Wang, L. Mining stress distribution and fault-slip behavior a case study of fault-influenced long wallcoal mining. *Energies* **2019**, *12*, 2494. [CrossRef]
3. Lei, G.W.; Yang, C.H.; Wang, G.B.; Chen, S.W.; Wei, X.; Huo, L. The development law and mechanical causes of fault influenced zone. *Chin. J. Rock Mech. Eng.* **2016**, *35*, 231–241.
4. Luo, H.; Li, Z.H.; Wang, A.W.; Xiao, Y.H. Study on the evolution law of stress field when approaching fault in deep mining. *J. Chin. Coal Soc.* **2014**, *39*, 322–327.
5. Lyu, P.F.; Bao, X.Y.; Lyu, G.; Chen, X.H. Research on Fault Activation Law in Deep Mining Face and Mechanism of Rockburst Induced by Fault Activation. *Adv. Civ. Eng.* **2020**, *2020*, 8854467.
6. Hu, X.Y.; Wang, L.G.; Lu, Y.L.; Yu, M. Analysis of insidious fault activation and water inrush from the mining floor. *Int. J. Min. Sci.* **2014**, *24*, 477–483. [CrossRef]
7. Ścigała, R.; Szafulera, K. Linear discontinuous deformations created on the surface as an effect of underground mining and local geological conditions-case study. *Bull. Eng. Geol. Environ.* **2020**, *79*, 2059–2068. [CrossRef]
8. Yu, Q.H.; Zhang, H.X.; Zhang, Y.J.; Deng, W.N.; Zhang, G.Y. Analysis of fault activation mechanism and influencing factors caused by mining. *J. Chin. Coal Soc.* **2019**, *44*, 18–30.
9. Zhang, N.B.; Zhao, S.K.; Deng, Z.G.; Li, H.T.; Wang, Y.; Qin, K. Mechanical instability mechanism of thrust fault under static and dynamic loading. *J. Min. Safety Eng.* **2019**, *36*, 1186–1192.
10. Yin, Y.Q.; Li, P.E.; Di, Y. Instability and jumping phenomenon of rock structure. *Chin. J. Rock Mech. Eng.* **2015**, *34*, 945–952.
11. Pan, Y.S. Study on Rockburst Initiation and Failure Propagation. Ph.D. Thesis, Tsinghua University, Beijing, China, 1999.
12. Islam, M.R.; Shinjo, R. Mining-induced fault reacti-vation associated with the main conveyor belt roadway and safety of the Barapukuria coal mine in Bangladesh: Constraints from BEM simulations. *Int. J. Coal Geol.* **2009**, *79*, 115–130. [CrossRef]
13. Jiang, J.Q.; Wu, Q.S.; Qu, H. Characteristic of mining stress evolution and activation of the reverse fault below thehard-thick strata. *J. Chin. Coal Soc.* **2015**, *40*, 115–130.
14. Sainoki, A.; Mitri, H.S. Effect of slip-weakening distance on selected seismic source parameters of min-ing-induced fault-slip. *Int. J. Rock Mech. Min. Sci.* **2015**, *73*, 115–122. [CrossRef]
15. Cai, W.; Dou, L.M.; Wang, G.F.; Hu, Y.W. Mechanism of fault reactivation and its induced coal burst caused by coal mining activities. *J. Min. Saf. Eng.* **2019**, *36*, 1193–1202.
16. Han, K.M.; Yu, Q.H.; Zhang, H.X.; Li, F.M. Mechanism of fault activation when mining on hanging-wall and foot-wall. *J. Chin. Coal Soc.* **2020**, *45*, 1327–1335.
17. Zuo, J.P.; Chen, Z.H.; Wang, H.W.; Liu, X.P.; Wu, Z.P. Experimental investigation on fault activation pattern under deep mining. *J. Chin. Coal Soc.* **2009**, *34*, 305–309.
18. Liu, C.; Li, S.G.; Cheng, C.; Xue, J.H. Activation characteristics analysis on concealed fault in the excavating coal roadway based on microseismic monitoring technique. *Int. J. Min. Sci. Technol.* **2017**, *27*, 883–887. [CrossRef]
19. Loginov, G.N.; Yaskevich, S.V.; Duchkov, A.A.; Serdyukov, A.S. Joint processing of surface and underground microseismic monitoring data in hard mineral mining. *J. Min. Sci.* **2015**, *51*, 944–950. [CrossRef]
20. Kurlenya, M.V.; Serdyukov, A.S.; Azarov, A.V.; Nikitin, A.A. Numerical modeling of wavefields of microseismic events in underground mining. *J. Min. Sci.* **2015**, *51*, 689–695. [CrossRef]
21. Jiang, F.X.; Liu, J.W.; Ye, G.X.; Li, W. Coupling study of microseismic monitoring and numerical simulationfor tectonic activation. *Chin. J. Rock Mech. Eng.* **2009**, *29*, 3590–3597.
22. Shen, B.; Yi, D.; Xun, L.; Mattvan, V.D.W.; Bongani, D.; Lu, C.; Onur, V.; Ismet, C. Monitoring and modelling stress state near major geological structures in an underground coal mine for coal burst assessment. *Int. J. Rock Mech. Min.* **2020**, *129*, 104294. [CrossRef]
23. Ghosh, G.K.; Sivakumar, C. Application of underground microseismic monitoring for ground failure and secure longwall coal mining operation: A case study in an Indian mine. *J. Appl. Geophys.* **2018**, *150*, 21–39. [CrossRef]
24. Cai, W.; Dou, L.M.; Si, G.Y.; Hu, Y.W. Fault-Induced Coal Burst Mechanism under Mining-Induced Static and Dynamic Stresses. *Engineering* **2021**, *7*, 306–334. [CrossRef]

25. Jiao, Z.H.; Zhao, Y.X.; Jiang, Y.D.; Wang, H.; Lu, Z.G.; Wang, X.Z. Fault damage induced by mining and its sensitivity analysis of influencing factors. *J. Chin. Coal Soc.* **2017**, *42*, 36–42.
26. Zhao, S.K. Experiments on the characteristics of thrust fault activation influenced by miningoperation. *J. Min. Safety Eng.* **2016**, *33*, 354–360.
27. Bradley, F.; Nicholas, V.; Mark, S.; Diederichs; Andrew, J.; Hyett; Allan, P. An in situ monitoring campaign of a hard rock pillar at great depth within a Canadian mine. *J. Rock Mech. Geotech.* **2020**, *12*, 427–448.
28. Naruse, H.; Uehara, H.; Deguchi, T.; Fujihashi, K.; Onishi, M.; Espinoza, R.; Pinto, M. Application of a distributed fibre optic strain sensing system to monitoring changes in the state of an underground mine. *Meas. Sci. Technol.* **2007**, *18*, 3202–3210. [CrossRef]
29. Serdyukov, S.; Azarov, A.; Dergach, P.; Duchkov, A. Equipment for microseismic monitoring of geodynamic processes in underground hard mineral mining. *J. Min. Sci.* **2015**, *51*, 634–640. [CrossRef]
30. Guo, Y.H.; Hou, K.P. In-situ Stress Measurement and Prediction Analysis of Rockburst in Deep Mining of Shizishan Copper Mine. *Electron. J. Geotech. Eng.* **2014**, *19*, 2513–2524.
31. Huang, X.; Xu, N.; Wei, W.; Xiao, P.; Dong, L.; Li, B. Instability of an intersecting fault-dyke system during deep rock excavation. *Int. J. Rock Mech. Min.* **2022**, *153*, 105087. [CrossRef]
32. Zhang, C.S.; Liu, N.; Zhu, H.C.; Chu, W.; Wu, J.Y. Time-dependent behavior of crack propagation and evaluation of control effect of jinping deep marble. *Chin. J. Rock Mech. Eng.* **2013**, *32*, 1964–1972.
33. Emilio, B.; Gianpiero, R. Lining structural monitoring in the new underground service of Naples (Italy). *Tunn. Undergr. Space Technol.* **2016**, *51*, 152–163.
34. Zhang, N.B.; Wang, J.D.; Zhao, S.K.; Yang, S.H.; Deng, Z.G.; Ding, C.H. Evaluation of coal bump risk in excavation roadway based on multi-point stress and displacement monitoring system. *J. China Coal Soc.* **2020**, *45*, 140–149.
35. Guo, Y.H. Study on the Regularity, Mechanism and Deformation Forecast of Rockmass Movement Induced by Caving Mining Steep Deposit in High Stress Area. Ph.D. Thesis, Kunming University of Science and Technology, Kunming, China, 2015.